Computing 78, 31–53 (2006)
Digital Object Identifier (DOI) 10.1007/s00607-006-0171-5

Computing
Printed in Austria

Computer Simulation of Compositional Flow Using Unstructured Control Volume Finite Element Methods

Z. Chen, **G. Huan**, Dallas, and **H. Wang**, Beijing

Received July 7, 2005; revised October 5, 2005
Published online: July 13, 2006

Abstract

In this paper, we study the computer simulation of gas cycling in a rich retrograde condensate reservoir. Two prediction cases are studied. The first case is gas cycling with constant sales gas removal, and the second case is cycling with some gas sales deferral to enhance pressure maintenance in the early life of this reservoir. In this problem the great majority of cycling takes place at pressure below the dew point pressure, indicating the need for modeling the compositional three-phase, multicomponent flow in the reservoir. This compositional model consists of Darcy's law for volumetric flow velocities, mass conservation for hydrocarbon components, thermodynamic equilibrium for mass interchange between phases, and an equation of state for saturations. The control volume finite element (CVFE) method on unstructured grids is used to discretize the model governing equations for the first time. Numerical experiments are reported for the benchmark problem of the third comparative solution project (CSP) organized by the society of petroleum engineers (SPE). The PVT (pressure-volume-temperature) data are based on a real fluid analysis.

AMS Subject Classifications: 35K60, 35K65, 76S05, 76T05.

Keywords: Compositional model, reservoir simulation, control volume finite element, unstructured grids, gas cycling, condensate reservoir, numerical experiments.

1. Introduction

The finite difference method has been widely used in the numerical simulation of fluid flow in porous media. However, this method causes numerical dispersion and grid orientation problems [9]. It also gives rise to difficulties in the treatment of complicated geometry and boundary conditions. To overcome these deficiencies, one has utilized the intrinsic grid flexibility of the finite element method [3], but this method does not conserve mass locally. Recently, the control volume finite element (CVFE) method has been developed to enforce such a conservation property [10]. In addition, recent interest on unstructured grid reservoir simulation has been rapidly increased because of improved geological modeling and new well drilling technology [1]. The CVFE is well suited to this purpose.

The CVFE method has been applied to the numerical simulation of the black oil model [12], [13], [21]. In the hydrocarbon system of this model, only two components are present: gas (mainly methane and ethane) and oil. In the compositional model under consideration, only the number of chemical species is *a priori* given,

and the number of phases and the composition of each phase in terms of the given species depend on the thermodynamical conditions and the overall concentration of each species. This general model incorporates compressibility, compositional effects, and mass interchange between phases. It consists of Darcy's law for volumetric flow velocities, mass conservation for hydrocarbon components, thermodynamic equilibrium for mass interchange between phases, and an equation of state for saturations. It models important hydrocarbon recovery processes such as natural depletion or gas cycling drive for gas condensate reservoirs and miscible flooding for volatile oil reservoirs. To understand complex thermodynamic and physical processes of multiphase, multicomponent flow in porous media, it has become increasingly important to simulate numerically such a realistic model.

A qualitative analysis of the compositional model was given in [6]. The mathematical structure of the differential system describing this model was studied, and numerical results were given for a one-dimensional version of this model in [20]. Numerical results for a three-dimensional compositional model were presented in [5] using finite differences. The CVFE method on unstructured grids is here used for the first time for the discretization of the compositional governing equations. As noted above, in addition to the intrinsic grid flexibility of the finite element method, the CVFE conserves mass locally (i.e., on each control volume). Moreover, it reduces grid orientation effects, is efficiently adapted in local grid refinement, and can easily handle faults, corner points, and slanted wells [18]. These features are extremely important in numerical reservoir simulation.

Fluid flow models in porous media involve large systems of nonlinear, coupled, time-dependent partial differential equations. An important problem in reservoir simulation is to develop stable, efficient, robust, and accurate solution methods for solving these coupled equations. Essentially, there are three types of solution methods in reservoir simulation: the IMPES (implicit in pressure and explicit in saturation), the fully implicit, and the sequential. The fully implicit solution method, which is also called the simultaneous solution method [8], solves all of the coupled nonlinear equations simultaneously. This method is stable and can take large time steps, while its stability is maintained. However, due to a large number of partial differential equations to solve for the compositional model, this solution method is computationally prohibitive, even on today's most powerful supercomputers. The sequential solution method [14] splits the coupled system of nonlinear governing equations of reservoir simulation up into individual equations and solves each of these equations separately and implicitly. This method is less stable but more efficient than the fully implicit method for the compositional model, and will be investigated in our future study for this model. In the present paper, by a careful choice of the primary unknowns an *iterative* IMPES solution method is employed to solve the system of the compositional governing equations. When the IMPES is used within a Newton-Raphson iteration, we call it the iterative IMPES. Numerical results are reported for the benchmark problem of the third comparative solution project (CSP) organized by the society of petroleum engineers (SPE), and show that this iterative IMPES method performs very well for problems of a moderate size.

2. Basic Differential Equations

We consider a compositional model under the assumptions that the flow process is isothermal (i.e., constant temperature), the components form at most three phases (e.g., water, oil, and gas), there is no mass interchange between the water phase and the hydrocarbon phases (i.e., the oil and gas phases), and the diffusive effects are neglected.

Let ϕ and $\mathbf{k}$ denote the porosity and permeability of a porous medium $\Omega \subset \Re^3$, and S_α, μ_α, p_α, $\mathbf{u}_\alpha$, and $k_{r\alpha}$ be the saturation, viscosity, pressure, volumetric velocity, and relative permeability of the α phase, $\alpha = w, o, g$, respectively. Also, let ξ_{io} and ξ_{ig} represent the molar densities of component i in the oil (liquid) and gas (vapor) phases, respectively, $i = 1, 2, \ldots, N_c$, where N_c is the number of components. The molar density of phase α is given by

$$\xi_\alpha = \sum_{i=1}^{N_c} \xi_{i\alpha}, \quad \alpha = o,\ g. \tag{2.1}$$

The mole fraction of component i in phase α is then defined by

$$x_{i\alpha} = \xi_{i\alpha}/\xi_\alpha, \quad 1, 2, \ldots, N_c,\ \alpha = o, g. \tag{2.2}$$

The total mass is conserved for each component, $i = 1, \ldots, N_c$:

$$\begin{aligned} &\frac{\partial(\phi\xi_w S_w)}{\partial t} + \nabla \cdot (\xi_w \mathbf{u}_w) = q_w, \\ &\frac{\partial(\phi[x_{io}\xi_o S_o + x_{ig}\xi_g S_g])}{\partial t} + \nabla \cdot (x_{io}\xi_o \mathbf{u}_o + x_{ig}\xi_g \mathbf{u}_g) = x_{io}q_o + x_{ig}q_g, \end{aligned} \tag{2.3}$$

where ξ_w is the molar density of water (that is the water mass density ρ_w in the present case) and q_α stands for the flow rate of phase α at wells. In Eq. (2.3), the volumetric velocity $\mathbf{u}_\alpha$ is given by Darcy's law:

$$\mathbf{u}_\alpha = -\frac{k_{r\alpha}}{\mu_\alpha}\mathbf{k}\left(\nabla p_\alpha - \rho_\alpha \wp \nabla z\right), \qquad \alpha = w,\ o,\ g, \tag{2.4}$$

where ρ_α is the mass density of the α-phase, $\wp$ is the magnitude of the gravitational acceleration, and z is the depth. The mass flow rates q_α of wells are given by Peaceman's formulas [16].

In addition to the differential equations (2.3) and (2.4), there are also algebraic constraints. The mole fraction balance implies that

$$\sum_{i=1}^{N_c} x_{io} = 1, \quad \sum_{i=1}^{N_c} x_{ig} = 1. \tag{2.5}$$

In the transport process, the saturation constraint reads

$$S_w + S_o + S_g = 1. \tag{2.6}$$

Finally, the phase pressures are related by capillary pressures

$$p_{cow} = p_o - p_w, \quad p_{cgo} = p_g - p_o. \tag{2.7}$$

Mass interchange between phases is characterized by the variation of mass distribution of each component in the oil and gas phases. As usual, these two phases are assumed to be in the phase equilibrium state at every moment. This is physically reasonable since the mass interchange between phases occurs much faster than the flow of porous media fluids. Consequently, the distribution of each hydrocarbon component into the two phases is subject to the condition of stable thermodynamic equilibrium, which is given by minimizing the Gibbs free energy of the compositional system [2], [6]:

$$f_{io}(p_o, x_{1o}, x_{2o}, \ldots, x_{N_co}) = f_{ig}(p_g, x_{1g}, x_{2g}, \ldots, x_{N_cg}), \tag{2.8}$$

where f_{io} and f_{ig} are the fugacity functions of the ith component in the oil and gas phases [7], [17], respectively, $i = 1, 2, \ldots, N_c$.

Equations (2.3)–(2.8) provide $2N_c + 9$ independent relations, differential or algebraic, for the $2N_c + 9$ dependent variables: $x_{io}, x_{ig}, \mathbf{u}_\alpha, p_\alpha$, and $S_\alpha, \alpha = w, o, g$, $i = 1, 2, \ldots, N_c$. With appropriate boundary and initial conditions, there is a closed differential system for these unknowns.

3. Iterative IMPES Solution Method

When the IMPES is used within a Newton-Raphson iteration, we call it the iterative IMPES, as mentioned.

3.1. Choice of Primary Variables

As discussed in the previous section, Eqs. (2.3)–(2.8) form a strongly coupled system of time-dependent, nonlinear differential equations and algebraic constraints. While there are $2N_c + 9$ equations for the same number of dependent variables, this system can be written in terms of $2N_c + 2$ primary variables, and other variables can be expressed as functions of them. The choice of these primary variables is very important. They must be carefully chosen so that main physical properties inherent in the governing equations and constraints are preserved, nonlinearity of and the coupling between the equations are weakened, and efficient numerical methods for the solution of the resulting system can be devised.

To simplify the expressions in Eq. (2.3), we introduce some notation. We utilize the potentials

$$\Phi_\alpha = p_\alpha - \rho_\alpha \wp z, \qquad \alpha = w, o, g. \tag{3.1}$$

Also, we use the total mass variable F of the hydrocarbon system [15], [23]

$$F = \xi_o S_o + \xi_g S_g, \tag{3.2}$$

and the mass fractions of oil and gas in this system

$$L = \xi_o S_o / F, \quad V = \xi_g S_g / F. \tag{3.3}$$

Note that $L + V = 1$. Next, instead of exploiting the individual mole fractions, we use the total mole fraction of the components in the hydrocarbon system

$$z_i = L x_{io} + (1 - L) x_{ig}, \qquad i = 1, 2, \ldots, N_c. \tag{3.4}$$

Then it is easy to see, using (2.5), (3.2), and (3.3), that

$$\sum_{i=1}^{N_c} z_i = 1, \tag{3.5}$$

and

$$x_{io} \xi_o S_o + x_{ig} \xi_g S_g = F z_i, \qquad i = 1, 2, \ldots, N_c. \tag{3.6}$$

Consequently, applying (2.4) and (3.1), the second equation of (2.3) becomes, $i = 1, 2, \ldots, N_c$,

$$\frac{\partial(\phi F z_i)}{\partial t} - \nabla \cdot \left(\mathbf{k} \left[\frac{x_{io} \xi_o k_{ro}}{\mu_o} \nabla \Phi_o + \frac{x_{ig} \xi_g k_{rg}}{\mu_g} \nabla \Phi_g \right] \right) = x_{io} q_o + x_{ig} q_g. \tag{3.7}$$

Adding the equations in (3.7) over i and exploiting (2.5) and (3.5) give

$$\frac{\partial(\phi F)}{\partial t} - \nabla \cdot \left(\mathbf{k} \left[\frac{\xi_o k_{ro}}{\mu_o} \nabla \Phi_o + \frac{\xi_g k_{rg}}{\mu_g} \nabla \Phi_g \right] \right) = q_o + q_g. \tag{3.8}$$

Equation (3.7) is the individual flow equation for the i-th component (say, $i = 1, 2, \ldots, N_c - 1$) and Eq. (3.8) is the global hydrocarbon flow equation.

To simplify the differential equations further, we define the transmissibilities

$$\mathbf{T}_\alpha = \frac{\xi_\alpha k_{r\alpha}}{\mu_\alpha} \mathbf{k}, \quad \mathbf{T}_{i\alpha} = \frac{x_{i\alpha} \xi_\alpha k_{r\alpha}}{\mu_\alpha} \mathbf{k}, \qquad \alpha = w, o, g, \ i = 1, 2, \ldots, N_c. \tag{3.9}$$

We now summarize the equations needed in the iterative IMPES. The equilibrium relation (2.8) is recast, $i = 1, 2, \ldots, N_c$,

$$f_{io}(p_o, x_{1o}, x_{2o}, \ldots, x_{N_c o}) = f_{ig}(p_o + p_{cg}, x_{1g}, x_{2g}, \ldots, x_{N_c g}). \tag{3.10}$$

Using (3.9), Eq. (3.7) becomes, $i = 1, 2, \ldots, N_c - 1$,

$$\frac{\partial(\phi F z_i)}{\partial t} = \nabla \cdot (\mathbf{T}_{io} \nabla \Phi_o + \mathbf{T}_{ig} \nabla \Phi_g) + x_{io} q_o + x_{ig} q_g. \tag{3.11}$$

Similarly, it follows from (3.8) that

$$\frac{\partial(\phi F)}{\partial t} = \nabla \cdot (\mathbf{T}_o \nabla \Phi_o + \mathbf{T}_g \nabla \Phi_g) + q_o + q_g. \tag{3.12}$$

Next, applying the first equation of (2.3) and (3.9) yields

$$\frac{\partial(\phi\xi_w S_w)}{\partial t} = \nabla\cdot(\mathbf{T}_w\nabla\Phi_w) + q_w. \tag{3.13}$$

Finally, using (3.2) and (3.3), the saturation state equation (2.6) becomes

$$F\left(\frac{L}{\xi_o} + \frac{1-L}{\xi_g}\right) + S = 1. \tag{3.14}$$

The differential system consists of the $2N_c + 2$ equations (3.10)–(3.14) for the $2N_c + 2$ primary unknowns: x_{io} (or x_{ig}), L (or V), z_i, F, $S = S_w$, and $p = p_o$, $i = 1, 2, \ldots, N_c - 1$.

3.2. The Iterative IMPES

Let $n > 0$ (an integer) refer to a time step. For any function v of spaceand time, we write $v^n(\cdot) = v(\cdot, t^n)$, and use $\bar{\delta}v$ to denote the time difference

$$\bar{\delta}v = v^{n+1} - v^n.$$

A time approximation at the $(n+1)$-th level for the system of equations (3.10)–(3.14) is given by, $i = 1, 2, \ldots, N_c$,

$$\begin{aligned}
&f_{io}(p_o^{n+1}, x_{1o}^{n+1}, x_{2o}^{n+1}, \ldots, x_{N_co}^{n+1}) = f_{ig}(p_g^{n+1}, x_{1g}^{n+1}, x_{2g}^{n+1}, \ldots, x_{N_cg}^{n+1}),\\
&\frac{1}{\Delta t}\bar{\delta}(\phi F z_i) = \nabla\cdot(\mathbf{T}_{io}^n\nabla\Phi_o^{n+1} + \mathbf{T}_{ig}^n\nabla\Phi_g^{n+1}) + x_{io}^{n+1}q_o^n + x_{ig}^{n+1}q_g^n,\\
&\frac{1}{\Delta t}\bar{\delta}(\phi F) = \nabla\cdot(\mathbf{T}_o^n\nabla\Phi_o^{n+1} + \mathbf{T}_g^n\nabla\Phi_g^{n+1}) + q_o^n + q_g^n,\\
&\frac{1}{\Delta t}\bar{\delta}(\phi\xi_w S) = \nabla\cdot(\mathbf{T}_w^n\nabla\Phi_w^{n+1}) + q_w^n,\\
&\left[F\left(\frac{L}{\xi_o} + \frac{1-L}{\xi_g}\right) + S\right]^{n+1} = 1,
\end{aligned} \tag{3.15}$$

where $\Delta t = t^{n+1} - t^n$. Observe that the transmissibilities and well terms in (3.15) are evaluated at the previous time level.

System (3.15) is nonlinear in the primary unknowns, and can be linearized via the Newton-Raphson iteration, for example. For function v, we set

$$v^{n+1,l+1} = v^{n+1,l} + \delta v,$$

where l refers to the number of Newton-Raphson's iteration and δv represents the increment in this iteration step. When no ambiguity occurs, we will write $v^{n+1,l+1}$ and $v^{n+1,l}$ by v^{l+1} and v^l, respectively (i.e., the superscript $n+1$ is omitted). Note that

$v^{n+1} \approx v^{l+1} = v^l + \delta v$, so $\bar{\delta} v \approx v^l - v^n + \delta v$. Using this approximation in system (3.15) yields, $i = 1, 2, \ldots, N_c$,

$$
\begin{aligned}
& f_{io}\left(p_o^{l+1}, x_{1o}^{l+1}, x_{2o}^{l+1}, \ldots, x_{N_c o}^{l+1}\right) = f_{ig}\left(p_g^{l+1}, x_{1g}^{l+1}, x_{2g}^{l+1}, \ldots, x_{N_c g}^{l+1}\right), \\
& \frac{1}{\Delta t}\left[(\phi F z_i)^l - (\phi F z_i)^n + \delta(\phi F z_i)\right] \\
& \qquad = \nabla \cdot \left(\mathbf{T}_{io}^n \nabla \Phi_o^{l+1} + \mathbf{T}_{ig}^n \nabla \Phi_g^{l+1}\right) + x_{io}^{l+1} q_o^n + x_{ig}^{l+1} q_g^n, \\
& \frac{1}{\Delta t}\left[(\phi F)^l - (\phi F)^n + \delta(\phi F)\right] = \nabla \cdot \left(\mathbf{T}_o^n \nabla \Phi_o^{l+1} + \mathbf{T}_g^n \nabla \Phi_g^{l+1}\right) + q_o^n + q_g^n, \\
& \frac{1}{\Delta t}\left[(\phi \xi_w S)^l - (\phi \xi_w S)^n + \delta(\phi \xi_w S)\right] = \nabla \cdot \left(\mathbf{T}_w^n \nabla \Phi_w^{l+1}\right) + q_w^n, \\
& \left[F\left(\frac{L}{\xi_o} + \frac{1-L}{\xi_g}\right) + S\right]^{l+1} = 1.
\end{aligned}
\tag{3.16}
$$

We expand the potentials in terms of the primary unknowns. Toward that end, we must identify these unknowns. If the gas phase dominates in the hydrocarbon system (e.g., $L < 0.5$), the primary unknowns will be x_{io}, L, z_i, F, S, and $p, i = 1, 2, \ldots, N_c - 1$. That is, the so-called $L - X$ iteration type is used. If the oil phase dominates (e.g., $L \geq 0.5$), the primary unknowns will be x_{ig}, V, z_i, F, S, and $p, i = 1, 2, \ldots, N_c - 1$, which corresponds to the $V - Y$ iteration type. As an example, we illustrate how to expand these potentials in terms of $\delta x_{io}, \delta L, \delta z_i, \delta F, \delta S$, and $\delta p, i = 1, 2, \ldots, N_c - 1$; a similar expansion can be performed for the $V - Y$ iteration type.

For the i-th component flow equation,

$$
\delta(\phi F z_i) = c_{ip}\delta p + c_{iF}\delta F + c_{iz}\delta z_i, \quad i = 1, 2, \ldots, N_c - 1, \tag{3.17}
$$

where

$$
c_{ip} = \phi^o c_R (F z_i)^l, \quad c_{iF} = (\phi z_i)^l, \quad c_{iz} = (\phi F)^l,
$$

with ϕ^o being the porosity at a reference pressure p^o and c_R the rock compressibility. For the global hydrocarbon flow equation,

$$
\delta(\phi F) = c_p \delta p + c_F \delta F, \quad c_p = \phi^o c_R F^l, \quad c_F = \phi^l. \tag{3.18}
$$

For the water flow equation,

$$
\delta(\phi \xi_w S) = c_{wp}\delta p + c_{wS}\delta S, \quad c_{wp} = \phi^o c_R (\xi_w S)^l + \left(\phi \frac{d\xi_w}{dp} S\right)^l, \quad c_{wS} = (\phi \xi_w)^l. \tag{3.19}
$$

In iterative IMPES, all the saturation functions ($k_{rw}, k_{ro}, k_{rg}, p_{cw}$, and p_{cg}), densities, and viscosities are evaluated at the saturation values of the previous time step in Newton-Raphson's iteration. The phase potentials are calculated by

$$
\Phi_\alpha^{l+1} = p^{l+1} + p_{c\alpha}^n - \rho_\alpha^n \wp z, \qquad \alpha = w, o, g, \tag{3.20}
$$

and the transmissibilities are computed by

$$\mathbf{T}_\alpha^n = \frac{\xi_\alpha^n k_{r\alpha}^n}{\mu_\alpha^n}\mathbf{k}, \quad \mathbf{T}_{i\alpha}^n = \frac{x_{i\alpha}^n \xi_\alpha^n k_{r\alpha}^n}{\mu_\alpha^n}\mathbf{k}, \qquad \alpha = w, o, g,\ i = 1, 2, \ldots, N_c. \tag{3.21}$$

It follows from (3.20) that

$$\Phi_\alpha^{l+1} = \Phi_\alpha^l + \delta p, \quad \alpha = w, o, g. \tag{3.22}$$

We now expand each of the equations in system (3.16). For this, we replace the derivatives in x_{ig} by those in the primary variables, $i = 1, 2, \ldots, N_c$. Applying relation (3.4), we see that

$$\frac{\partial x_{ig}}{\partial x_{io}} = \frac{L}{L-1}, \quad \frac{\partial x_{ig}}{\partial z_i} = \frac{1}{1-L}, \quad \frac{\partial x_{ig}}{\partial L} = \frac{x_{io} - x_{ig}}{L-1}, \quad i = 1, 2, \ldots, N_c.$$

Consequently, the chain rule implies

$$\begin{aligned}
&\frac{\partial}{\partial x_{io}} = \frac{\partial x_{ig}}{\partial x_{io}}\frac{\partial}{\partial x_{ig}} = \frac{L}{L-1}\frac{\partial}{\partial x_{ig}}, \quad \frac{\partial}{\partial z_i} = \frac{\partial x_{ig}}{\partial z_i}\frac{\partial}{\partial x_{ig}} = \frac{1}{1-L}\frac{\partial}{\partial x_{ig}},\\
&\frac{\partial}{\partial L} = \frac{\partial x_{ig}}{\partial L}\frac{\partial}{\partial x_{ig}} = \frac{x_{io} - x_{ig}}{L-1}\frac{\partial}{\partial x_{ig}}.
\end{aligned}$$

Thus, after using (2.5) and (3.5) to eliminate $x_{N_c o}$ and z_{N_c}, the first equation in (3.16) can be expanded as follows:

$$\begin{aligned}
&\sum_{j=1}^{N_c-1}\left\{\left(\frac{\partial f_{io}}{\partial x_{jo}}\right)^l - \left(\frac{\partial f_{io}}{\partial x_{N_c o}}\right)^l + \frac{L^l}{1-L^l}\left[\left(\frac{\partial f_{ig}}{\partial x_{jg}}\right)^l - \left(\frac{\partial f_{ig}}{\partial x_{N_c g}}\right)^l\right]\right\}\delta x_{jo}\\
&\quad + \frac{1}{1-L^l}\sum_{j=1}^{N_c}\left(\frac{\partial f_{ig}}{\partial x_{jg}}\left(x_{jo} - x_{jg}\right)\right)^l \delta L\\
&= f_{ig}^l - f_{io}^l + \left[\left(\frac{\partial f_{ig}}{\partial p}\right)^l - \left(\frac{\partial f_{io}}{\partial p}\right)^l\right]\delta p\\
&\quad + \frac{1}{1-L^l}\sum_{j=1}^{N_c-1}\left[\left(\frac{\partial f_{ig}}{\partial x_{jg}}\right)^l - \left(\frac{\partial f_{ig}}{\partial x_{N_c g}}\right)^l\right]\delta z_j,
\end{aligned} \tag{3.23}$$

where, for $i = 1, 2, \ldots, N_c$,

$$f_{io}^l = f_{io}(p_o^l, x_{1o}^l, x_{2o}^l, \ldots, x_{N_c o}^l), \quad f_{ig}^l = f_{ig}(p_g^l, x_{1g}^l, x_{2g}^l, \ldots, x_{N_c g}^l).$$

Equation (3.23) is used to solve for $(\delta x_{1o}, \delta x_{2o}, \ldots, \delta x_{(N_c-1)o}, \delta L)$ in terms of $(\delta z_1, \delta z_2, \ldots, \delta z_{N_c-1}, \delta p)$. Note that this equation is linear in $(\delta x_{1o}, \delta x_{2o}, \ldots, \delta x_{(N_c-1)o}, \delta L)$.

Next, applying (3.17) and (3.22), from the second equation in (3.16) it follows that, $i = 1, 2, \ldots, N_c - 1$,

$$\begin{aligned}\frac{1}{\Delta t}\left[(\phi F z_i)^l - (\phi F z_i)^n + c_{ip}\delta p + c_{iF}\delta F + c_{iz}\delta z_i\right] \\ = \nabla\cdot(\mathbf{T}_{io}^n\nabla\Phi_o^l + \mathbf{T}_{ig}^n\nabla\Phi_g^l) + \nabla\cdot\left(\left(\mathbf{T}_{io}^n + \mathbf{T}_{ig}^n\right)\nabla(\delta p)\right) \\ + \left(x_{io}^l + \delta x_{io}\right)q_o(\delta p) + \left(x_{ig}^l + \delta x_{ig}\right)q_g(\delta p).\end{aligned} \tag{3.24}$$

Equation (3.24) is solved for $(\delta z_1, \delta z_2, \ldots, \delta z_{N_c-1})$ in terms of $(\delta F, \delta p)$. Similarly, from the third equation in (3.16) we see that

$$\begin{aligned}\frac{1}{\Delta t}\left[(\phi F)^l - (\phi F)^n + c_p\delta p + c_F\delta F\right] \\ = \nabla\cdot\left(\mathbf{T}_o^n\nabla\Phi_o^l + \mathbf{T}_g^n\nabla\Phi_g^l\right) + \nabla\cdot\left(\left(\mathbf{T}_o^n + \mathbf{T}_g^n\right)\nabla(\delta p)\right) + q_o(\delta p) + q_g(\delta p),\end{aligned} \tag{3.25}$$

which is employed to solve for δF in terms of δp. From the fourth equation in (3.16), (3.19), and (3.22), we have

$$\begin{aligned}\frac{1}{\Delta t}\left[(\phi\xi_w S)^l - (\phi\xi_w S)^n + c_{wp}\delta p + c_{wS}\delta S\right] \\ = \nabla\cdot\left(\mathbf{T}_w^n\nabla\Phi_w^l\right) + \nabla\cdot\left(\mathbf{T}_w^n\nabla(\delta p)\right) + q_w(\delta p).\end{aligned} \tag{3.26}$$

Equation (3.26) is utilized to obtain δS in terms of δp,

Note that

$$\frac{1}{\xi_\alpha} = \frac{Z_\alpha(p_\alpha, x_{1\alpha}, x_{2\alpha}, \ldots, x_{N_c\alpha})RT}{p_\alpha}, \qquad \alpha = o, g.$$

Then, applying (2.5) and (3.5), it follows from the last equation in (3.16) that

$$\begin{aligned}&\left(\frac{FLRT}{p}\right)^l\sum_{j=1}^{N_c-1}\left\{\left(\frac{\partial Z_o}{\partial x_{jo}}\right)^l - \left(\frac{\partial Z_o}{\partial x_{N_co}}\right)^l - \left[\left(\frac{\partial Z_g}{\partial x_{jg}}\right)^l - \left(\frac{\partial Z_g}{\partial x_{N_cg}}\right)^l\right]\right\}\delta x_{jo} \\ &\quad + \left(\frac{FRT}{p}\right)^l\left[Z_o - Z_g - \sum_{j=1}^{N_c}\left(\frac{\partial Z_g}{\partial x_{jg}}\left(x_{jo} - x_{jg}\right)\right)^l\right]\delta L \\ &\quad + \left(\frac{FRT}{p}\right)^l\sum_{j=1}^{N_c-1}\left\{\left(\frac{\partial Z_g}{\partial x_{jg}}\right)^l - \left(\frac{\partial Z_g}{\partial x_{N_cg}}\right)^l\right\}\delta z_j \\ &\quad + \left(\frac{RT}{p}\left(LZ_o + (1-L)Z_g\right)\right)^l\delta F + \delta S \\ &\quad + \left(\frac{FRT}{p}\left[L\frac{\partial Z_o}{\partial p} - \frac{LZ_o}{p} + (1-L)\frac{\partial Z_g}{\partial p} - \frac{(1-L)Z_g}{p}\right]\right)^l\delta p \\ &= 1 - \left(F\left[\frac{L}{\xi_o} + \frac{1-L}{\xi_g}\right] + S\right)^l.\end{aligned} \tag{3.27}$$

After substitution of δx_{jo}, δL, δz_j, δF, and δS, $j = 1, 2, \ldots, N_c - 1$ into (3.27) using Eqs. (3.23)–(3.26), the resulting equation will become the pressure equation, which, together with the well control equations, is implicitly solved for δp. The CVFE introduced in the next section is applied to the discretization of equations (3.23)–(3.27) in space.

In summary, the iterative IMPES for the compositional model has following features:

- The difference between the iterative IMPES and the classical IMPES is that the iterative IMPES is used within each Newton-Raphson iteration loop, while the classical one is utilized before the Newton-Raphson iteration.
- The saturation constraint equation is used to solve implicitly for pressure p.
- The equilibrium relation is solved for $(x_{1o}, x_{2o}, \ldots, x_{(N_c-1)o}, L)$.
- The hydrocarbon component flow equations are utilized to obtain explicitly for $(z_1, z_2, \ldots, z_{N_c-1})$.
- The global hydrocarbon flow equation is exploited to solve explicitly for F.
- The water flow equation is explicitly solved for S.
- Relation (3.4) generates $(x_{1g}, x_{2g}, \ldots, x_{N_c g})$.

4. Numerical Results

This simulation problem is chosen from the benchmark problem of the third CSP [11]. Nine companies participated in that comparison project. It is a study of gas cycling in a rich retrograte condensate reservoir. Two prediction cases are considered. The first case is gas cycling with constant sales gas removal, and the second case is cycling with some gas sales deferral to enhance pressure maintenance in the early life of the reservoir. The data are taken from [11]. The specification of the reservoir model is presented in Tables 1–5, where k_h and k_v denote the horizontal and vertical permeabilities, respectively. A reservoir grid with $9 \times 9 \times 4$ is shown in Fig. 1, and it is diagonally symmetrical, indicating that it would be possible to simulate half of this reservoir. We chose to model the full reservoir. Also, the reservoir layers are homogeneous and have a constant porosity, but there are permeability and thickness variations between layers, a factor leading to unequal sweepout. The two-well pattern is arbitrary and is employed to allow for some retrograde condensation without significant revaporization by recycling gas to simulate what occurs in sweep-inaccessable parts of a real reservoir.

Due to the layer structure in the vertical direction of the reservoir under consideration, we divide its domain into hexagonal prisms, i.e., hexagons in the horizontal plane and rectangles in the vertical direction, as seen in Fig. 2; also see Fig. 3 for a planar view of the grid. The initial conditions, the location of the gas-water contact, and the capillary pressure data produce a water-gas transition zone extending to the pay zones. However, the very small compressibility and water volume make water quite insignificant for the present problem. Relative permeability data are used under the assumption that the phase relative permeability function depends only on

Table 1. Reservoir grid data

$NX = NY = 9$, $NZ = 4$; $DX = DY = 293.3$ ft
$DZ = 30, 30, 50, 50$ ft; Datum=7,500 ft. (subsurface)
Porosity: 0.13 (at initial reservoir pressure)
Gas-water contact: 7,500 ft; S_w at contact: 1.0
p_{cgw} at contact: 0.0 psi; initial pressure at contact: 3,550 psia
Water density at contact: 63.0 lb/cu ft; c_w=3.0E-6 psi^{-1}
Formation water viscosity: 0.78 cp; Rock compressibility: 4.0E-6 psi^{-1}

Table 2. Reservoir model description

Layer	Thickness (ft)	k_h (md)	k_v (md)	Depth to center (ft)
1	30	130	13	7.330
2	30	40	4	7.360
3	50	20	2	7.400
4	50	150	15	7.450

Table 3. Saturation function data

Phase saturation	k_{rg}	k_{ro}	k_{rw}	p_{cgw} (psi)	p_{cgo} (psi)
0.00	0.00	0.00	0.00	> 50	0
0.04	0.005	0.00	0.00	> 50	0
0.08	0.013	0.00	0.00	> 50	0
0.12	0.026	0.00	0.00	> 50	0
0.16	0.040	0.00	0.00	50	0
0.20	0.058	0.00	0.002	32	0
0.24	0.078	0.00	0.010	21	0
0.28	0.100	0.005	0.020	15.5	0
0.32	0.126	0.012	0.033	12.0	0
0.36	0.156	0.024	0.049	9.2	0
0.40	0.187	0.040	0.066	7.0	0
0.44	0.222	0.060	0.090	5.3	0
0.48	0.260	0.082	0.119	4.2	0
0.52	0.300	0.112	0.150	3.4	0
0.56	0.348	0.150	0.186	2.7	0
0.60	0.400	0.196	0.227	2.1	0
0.64	0.450	0.250	0.277	1.7	0
0.68	0.505	0.315	0.330	1.3	0
0.72	0.562	0.400	0.390	1.0	0
0.76	0.620	0.513	0.462	0.7	0
0.80	0.680	0.650	0.540	0.5	0
0.84	0.740	0.800	0.620	0.4	0
0.88	–	–	0.710	0.3	0
0.92	–	–	0.800	0.2	0
0.96	–	–	0.900	0.1	0
1.00	–	–	1.000	0.0	0

its own phase saturation. Oil is immobile to 24% saturation, and k_{rg} is reduced from 0.74 to 0.4 as condensate builds to this saturation with irreducible water present.

Production is separator gas rate controlled. Liquid production through multistage separation is to be predicted. The separator train is given, and the primary separator pressure depends on reservoir pressure as shown in Table 5. Sales gas is removed

Table 4. Production, injection, and sales data

Production	Location: I=J=7; perforations: K=3,4; radius: $r_w = 1$ ft; rate: 6,200 Mscf/D (gas rate); min p_{bh}, 500 psi
Injection	Location: I=J=1; perforations: K=1,2; radius: $r_w = 1$ ft; rate: separator rate-sales rate; max p_{bh}: 4,000 psi
Sales rate for case 1	Constant sales rate to blowdown: $0 < t < 10$ yr, 1,500 Mscf/D; $t > 10$ yr, all produced gas to sales
Sales rate for case 2	Deferred sales: $0 < t < 5$ yr, 500 Mscf/D; $5 < t < 10$ yr, 2,500 Mscf/D; $t > 10$ yr, all produced gas to sales

Table 5. Separator pressures and temperatures

Separator	Pressure (psia)	Temperature (°F)
Primary	815	80
Primary	315	80
Second stage	65	80
Stock tank	14.7	60

Primary separation at 815 psia until reservoir pressure (at datum) falls below 2,500 psia; then switch to primary separation at 315 psia

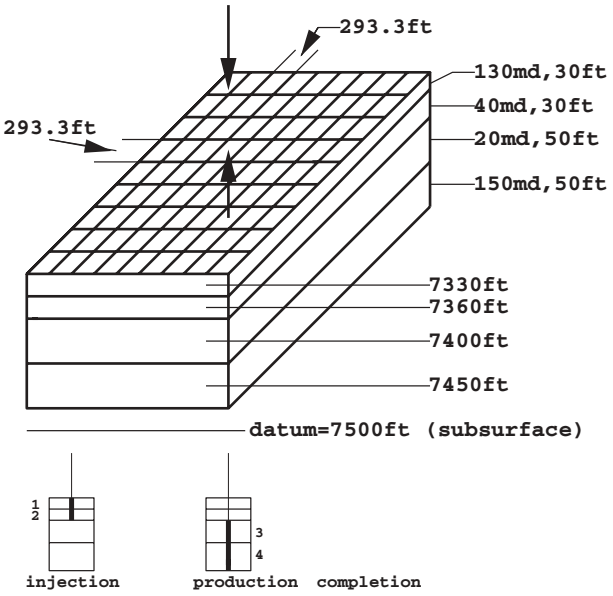

Fig. 1. A reservoir domain

from the bulked separator gas, and the remaining gas is recycled. Volumetrically, the two cases under consideration provide for exactly the same amount of recycling gas to be reinjected over the cycling period (10 years), but more gas is recycled in the critical early years in the second case. Blowdown (all gas to sales) starts at the end of the tenth year of cycling, and simulations are run up to 15 years or 1,000 psi

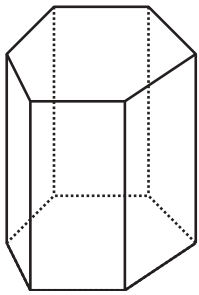

Fig. 2. A hexagonal prism

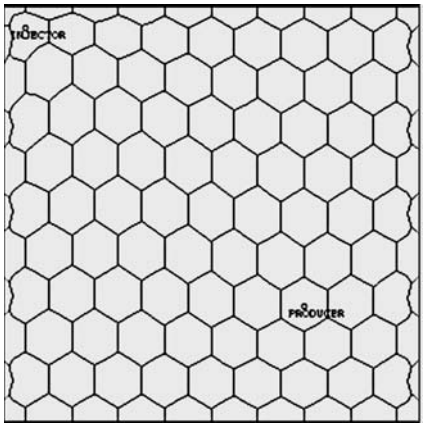

Fig. 3. A planar view of the grid

average reservoir pressure, whichever occurs first. The simulations are initialized at pressure about 100 psi above the dew point pressure 3, 443 psia.

The entire simulation study is divided in two stages:

- PVT phase behavior study to obtain accurate EOS parameters and prediction results.
- Reservoir simulation study of the compositional flow using the CVFE.

4.1. PVT Phase Behavior Study

4.1.1. PVT Data

The measured PVT data can be found in [4]. These data include hydrocarbon sample analysis, constant composition expansion data, constant volume depletion data, and swelling data of four mixtures of reservoir gas with lean gas.

4.1.2. PVT Study for Matching the PVT Data

The PVT study includes:

- Splitting C_{7+};
- Pseudo-grouping;
- Constant composition expansion and constant volume depletion;
- Swelling tests;
- Critical parameters at the formation and separator conditions for compositional modeling.

The heavy C_{7+} component is split into three components, HC_1, HC_2, and HC_3, to enhance the accuracy of PVT data matching. The mole fractions, molecular weights, and specific gravity of these components are stated in Table 6.

We use a pseudo-grouping approach to group components. The purpose of pseudo-grouping is to reduce the number of components involved in compositional modeling. These pseudo-components are described in Table 7.

Detailed matches of the PVT data are displayed in Figs. 4–7. Figure 4 shows pressure-volume data in constant composition expansion of the reservoir gas at 200°F. Figure 5 indicates retrograde condensate during constant volume depletion. Liquid yield by multistage surface separation in reservoir gas produced by constant volume depletion is displayed in Fig. 6. The results of swelling of reservoir gas with increasing the dew point pressure of injected lean gas are given in Fig. 7. There are very good agreements between the laboratory and computed PVT data.

Finally, Tables 8–11 give a summary for the characterization data and binary interaction coefficients of the components at the formation and separator conditions.

4.2. Reservoir Simulation Study

The initial fluids in-place using multistage separation are given below:

Wet gas (Bscf): 25.774, Dry gas (Bscf): 23.246, Stock tank oil (MMstb): 3.450.

Simulation results for the compositional model considered are given in Figs. 8–14. The time step size used in the iterative IMPES is about 30 days (in the first few time steps, it is smaller). Our compositional simulator can use either the ORTHOMIN (orthogonal minimum residual) [22] or GMRES (generalized minimum residual) [19] Krylov subspace methods, with incomplete LU factorization preconditioners, as the linear solver.

Table 6. HC_1, HC_2, and HC_3

Component	Mole fraction	Molecular weights	Specific gravity
HC_1	0.05011	118.44	0.74985
HC_2	0.01340	193.95	0.81023
HC_3	0.00238	295.30	0.86651

Table 7. Pseudo-grouping of components

Pseudo-component	P_1	P_2	P_3	P_4	P_5	P_6	P_7
Natural component	C_1, N_2	C_2, CO_2	C_3, C_4	C_5, C_6	HC_1	HC_2	HC_3
Mole fraction	0.6793	0.0990	0.1108	0.0450	0.05011	0.0134	0.00238
Molecular weights	16.38	31.77	50.64	77.78	118.44	193.95	295.30

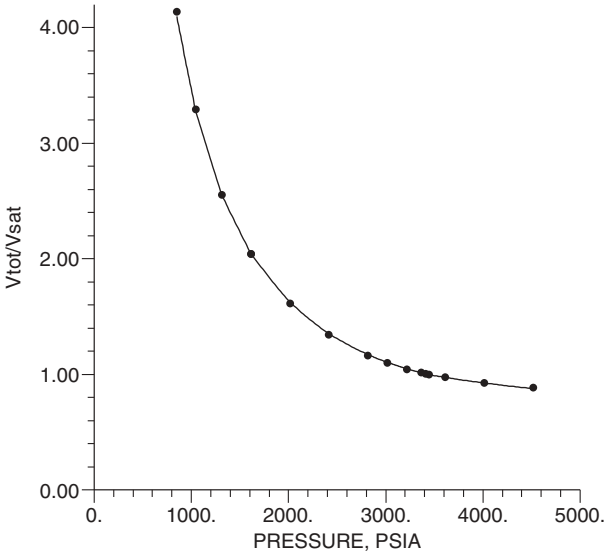

Fig. 4. Pressure-volume relation of reservoir fluid at 200° F – Constant composition expansion; the dotted line is laboratory and the solid is computed

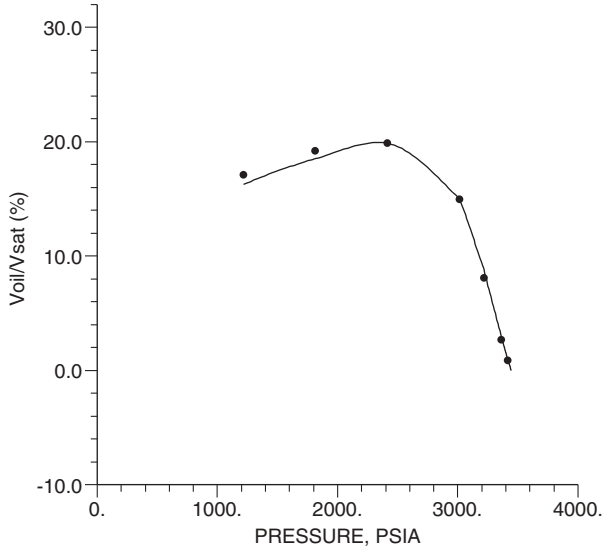

Fig. 5. Retrograde condensate during constant volume gas depletion at 200° F; the dotted line is laboratory and the solid is computed

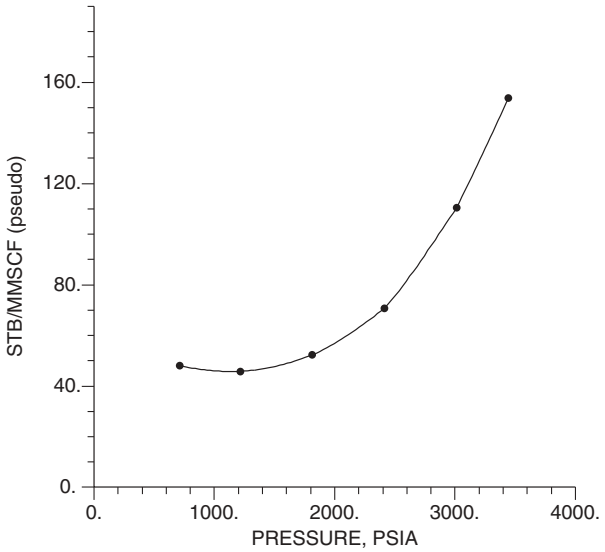

Fig. 6. Three-stage separator yield during constant volume gas depletion at 200° F; the dotted line is laboratory and the solid is computed

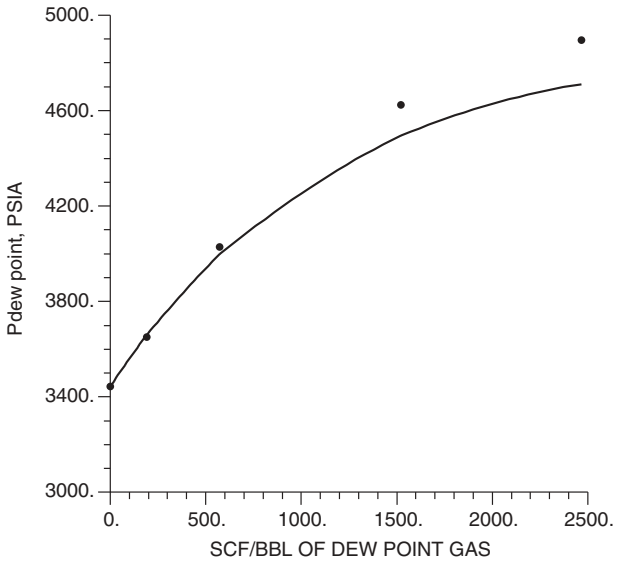

Fig. 7. Dew point pressure vs. cumulative gas injected during swelling with lean gas at 200° F; the dotted line is laboratory and the solid is computed

Stock-tank oil rates for the first and second cases and the corresponding cumulative liquid production for these cases at the final simulation time of 15 years are shown in Figs. 8–11. Incremental stock-tank oil produced by gas-sales deferral (the second case minus the first), and oil saturations are given in Figs. 12–14. Primary separator

Table 8. Characterization data of components at the formation conditions

Pseudo components	Z_c	P_c (psia)	T_c (°F)	Molecular weight	Acentric ω	Ω_a	Ω_b
P_1	0.28968	667.96	−119.11	16.38	0.00891	0.34477208	0.06328161
P_2	0.28385	753.82	90.01	31.77	0.11352	0.52197368	0.09982480
P_3	0.27532	586.26	252.71	50.64	0.17113	0.51497212	0.10747888
P_4	0.26699	469.59	413.50	77.78	0.26910	0.41916871	0.09345540
P_5	0.27164	410.14	605.99	118.44	0.34196	0.48594317	0.07486045
P_6	0.23907	260.33	795.11	193.95	0.51730	0.57058309	0.10120595
P_7	0.22216	183.92	988.26	295.30	0.72755	0.45723552	0.07779607

Table 9. Binary interaction coefficients at the formation conditions

components	P_1	P_2	P_3	P_4	P_5	P_6	P_7
P_1	0.0						
P_2	0.000622	0.0					
P_3	−0.002471	−0.001540	0.0				
P_4	0.011418	0.010046	0.002246	0.0			
P_5	−0.028367	0.010046	0.002246	0.0	0.0		
P_6	−0.100000	0.010046	0.002246	0.0	0.0	0.0	
P_7	0.206868	0.010046	0.002246	0.0	0.0	0.0	0.0

Table 10. Characterization data of components at the separator conditions

Pseudo components	Z_c	P_c (psia)	T_c (°F)	Molecular weight	Acentric ω	Ω_a	Ω_b
P_1	0.28968	667.96	−119.11	16.38	0.00891	0.50202385	0.09960379
P_2	0.28385	753.82	90.01	31.77	0.11352	0.45532152	0.08975547
P_3	0.27532	586.26	252.71	50.64	0.17113	0.46923415	0.08221724
P_4	0.26699	469.59	413.50	77.78	0.26910	0.58758251	0.08178213
P_5	0.27164	410.14	605.99	118.44	0.34196	0.55567652	0.06715680
P_6	0.23907	260.33	795.11	193.95	0.51730	0.49997263	0.07695341
P_7	0.22216	183.92	988.26	295.30	0.72755	0.45723552	0.07779607

Table 11. Binary interaction coefficients at the separator conditions

Components	P_1	P_2	P_3	P_4	P_5	P_6	P_7
P_1	0.0						
P_2	0.000622	0.0					
P_3	−0.002471	−0.001540	0.0				
P_4	0.011418	0.010046	0.002246	0.0			
P_5	0.117508	0.010046	0.002246	0.0	0.0		
P_6	0.149871	0.010046	0.002246	0.0	0.0	0.0	
P_7	0.112452	0.010046	0.002246	0.0	0.0	0.0	0.0

switchout occurs late in the cycling phase (10 years). The predicted surface oil rate is closely correlated with the liquid yield predictions shown in Fig. 6.

As noted earlier, the first case is gas cycling with constant sales gas removal, while the second case is cycling with some gas sales deferral to enhance pressure maintenance in the early life of the reservoir. The total sales gas removal is the same for

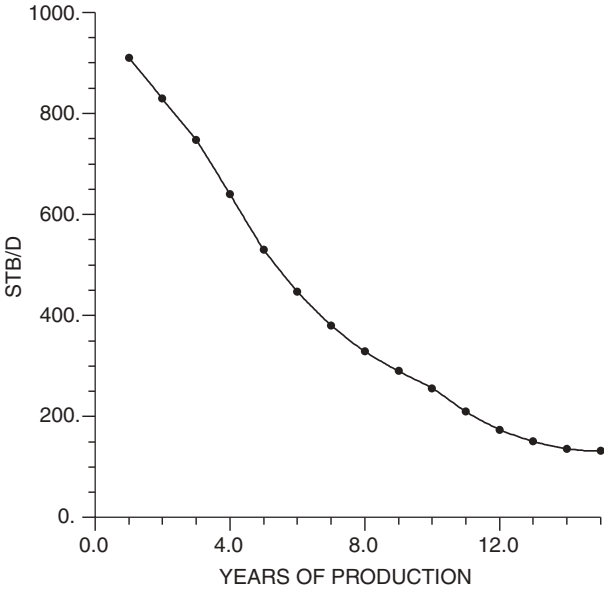

Fig. 8. Stock-tank oil production rate in case 1

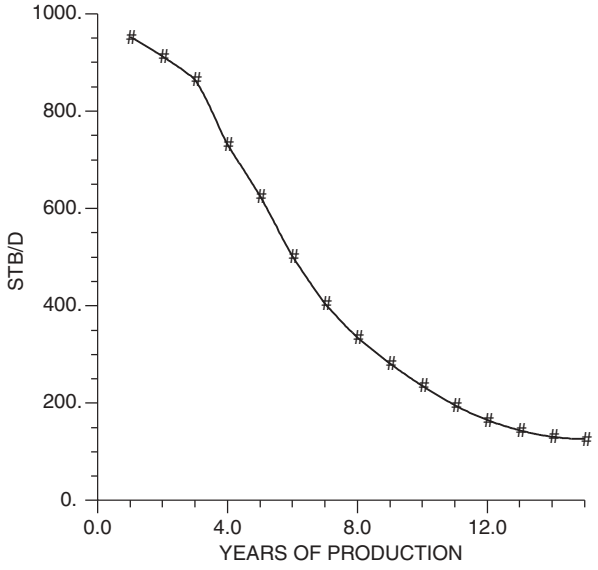

Fig. 9. Stock-tank oil production rate in case 2

the two cases; the difference lies in the way sales gas is removed in the first ten years (see Table 4). For a gas condensate reservoir, decreasing the occurring of retrograde condensate phenomena leads to less loss of heavy hydrocarbon components and more production of oil.

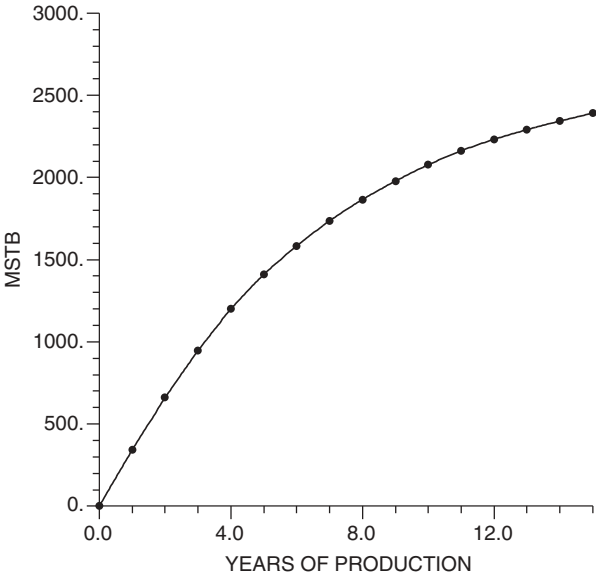

Fig. 10. Cumulative stock-tank oil production in case 1

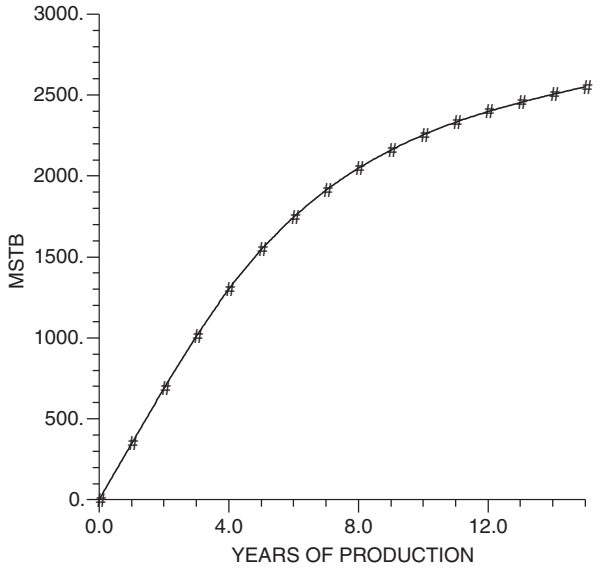

Fig. 11. Cumulative stock-tank oil production in case 2

Figure 12 gives incremental stock-tank oil produced by gas-sales deferral. In the peak of this curve (at the eighth year), the cumulative stock-tank oil produced by the second case is 182 Mstb more than that by the first case (i.e., 9.76% increase). At the final production time (the 15th year), the increase is down to 159 Mstb (6.65%). This phenomenon can be seen from the observation that after injection of recycle

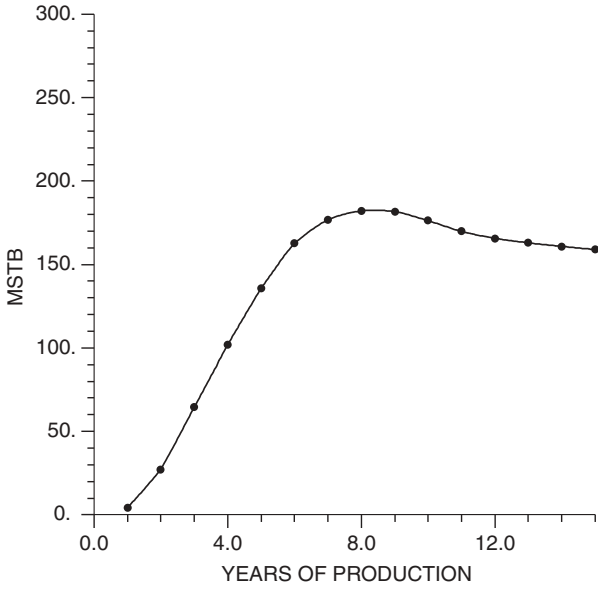

Fig. 12. Incremental stock-tank oil produced by gas-sales deferral (case 2 minus case 1)

gas stops, liquid production is due to depletion and the heavy end fractions vaporize into the vapor phase and are produced.

Figures 13 and 14 give the oil saturation at the grid block (7,7,4) for these two cases, respectively. From these two figures, we see that the oil saturation in the second case is smaller than that in the first case. This shows that the retrograde condensate phenomenon in the second occurs less than that in the first.

Compared with those presented in [11], the numerical results in Figs. 8–14 show that our numerical scheme performs very well. In fact, our stock-tank oil rate and corresponding cumulative production are close to the respective averaged values of those provided by nine companies in [11]. In our numerical scheme for the compositional simulation, the treatment of crossing "bubble points" and "dew points" in Newton-Raphson's iterations is very accurate, which leads to a very accurate computation of Jacobian matrices when the flow changes from three-phase to two-phase or vice versa. Our scheme also utilizes an accurate post-processing technique for checking consistency of the solution variables (F, L) with the natural variables (S_o, S_g) after the Newton-Raphson iterations. Through comparisons with other simulators and applications to real fluid analyses, we believe that our compositional simulator is a reliable, accurate, and fast simulator.

5. Concluding Remarks

We have developed an iterative IMPES solution approach to the numerical simulation of three-dimensional, three-phase, multicomponent compositional flow in

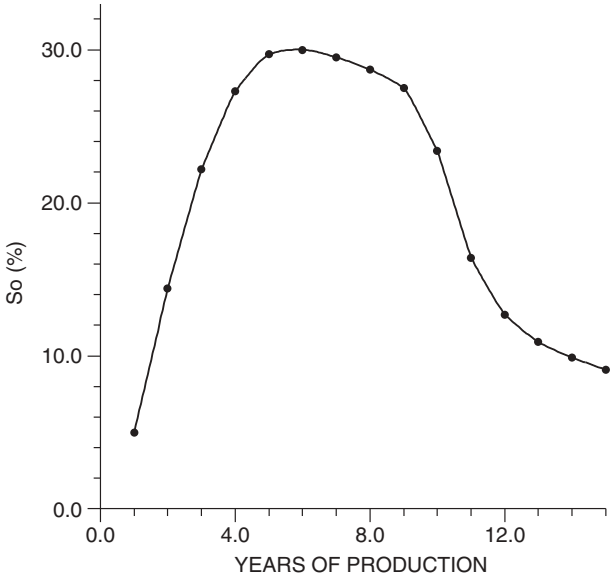

Fig. 13. Oil saturation in grid block (7,7,4) in case 1

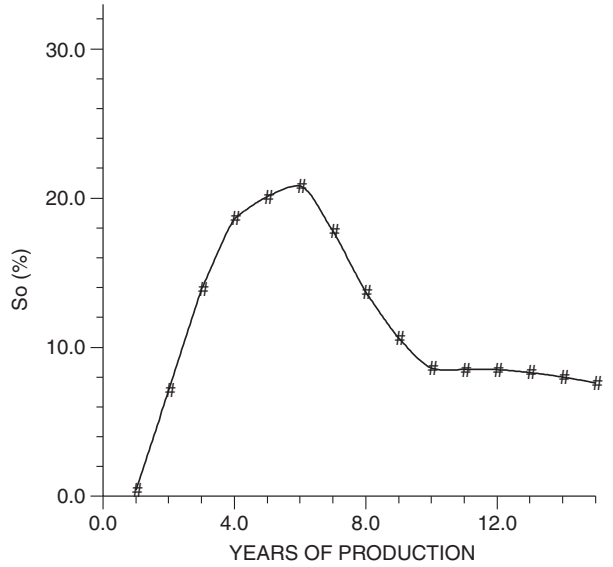

Fig. 14. Oil saturation in grid block (7,7,4) in case 2

porous media. The CVFE method on unstructured grids has been employed for the discretization of the governing equations of this compositional model. Numerical experiments have been presented for the benchmark problem of the third CSP, and have shown that the iterative IMPES approach performs very well for this problem of a moderate size. To simulate accurately the process of recycle gas injection in

a gas condensate reservoir using a compositional model, from our experience the following factors are very important:

- Through a PVT data match of the retrograde condensate curve during constant volume depletion, one is able to predict an accurate change of the reservoir oil saturation in the process of a pressure decrease.
- Through a PVT data match of swelling tests, one is able to see that the increase of the dew point pressure after injection of recycle gas can lead to the transfer of heavy hydrocarbon components in the thermodynamic equilibrium from the liquid phase to the vapor phase and to the production of these components at production wells, thus increasing their production.
- In compositional simulation, it is necessary to input two sets of critical PVT data; one set is in high pressure and is used for simulation of a reservoir flow process, while another set is in lower pressure and is used for simulation of a separator process. The efficiency of enhanced oil recovery depends on the accuracy of separator simulation.
- The simulations in Sect. 5 have been performed on an SGI Power Indigo with 1 GB RAM, and the CPU time for the present compositional problem at the final time of 15 years is about 39 seconds.

The CVFE method can be easily employed in a wide range of unstructured reservoir simulations (e.g., local grid refinement, horizontal well simulation, hybrid grids, and fault treatment). This paper provides a basis using this method for the compositional modeling. The nature of any IMPES solution approach restricts the time step size. To improve the efficiency of this approach for large-scale problems, we are investigating a sequential solution approach for the computation of the compositional model. In the sequential approach, the global hydrocarbon and water flow equations will be solved implicitly in pressure, saturation, and composition.

References

[1] Aavatsmark, I., Barkve, T., Boe, O., Mannseth, T.: Discretization on unstructured grids for inhomogeneous anisotropic media. Part II: Discussion and numerical results. SIAM J. Sci. Comput. *19*, 1717–1736 (1998).
[2] Bear, J.: Dynamics of fluids in porous media. New York: Dover 1972.
[3] Chen, Z., Ewing, R. E., Shi Z.-C. (eds.): Numerical treatment of multiphase flows in porous media. Lecture Notes in Physics, Vol. 552. Heidelberg: Springer 2000.
[4] Chen, Z., Huan, G., Ma, Y.: Computational methods for multiphase flows in porous media. Computational Science and Engineering Series, Vol. 2. Philadelphia, PA: SIAM 2006.
[5] Chen, Z., Huan, G., Wang, H.: Simulation of a compositional model for multiphase flow in porous media. Numer. Meth. Partial Diff. Equ. *21*, 726–741 (2005).
[6] Chen, Z., Qin, G., Ewing, R. E.: Analysis of a compositional model for fluid flow in porous media. SIAM J. Appl. Math. *60*, 747–777 (2000).
[7] Coats, K.-H.: An equation of state compositional model. Soc. Pet. Eng. J. *20*, 363–376 (1980).
[8] Douglas, J. Jr., Peaceman, D. W., Rachford, H. H. Jr.: A method for calculating multi-dimensional immiscible displacement. Trans. SPE of AIME *216*, 297–306 (1959).
[9] Ewing, R. E. (ed.): The mathematics of reservoir simulation. Philadelphia: SIAM 1983.
[10] Fung, L. S., Hiebert, A. D., Nghiem, L.: Reservoir simulation with a control volume finite element method, SPE 21224. 11th SPE Symp. on Reservoir Simulation, Anaheim, February 17–20, 1991.
[11] Kenyon, D. E., Behie, A.: Third SPE comparative solution project: Gas cycling of retrograde condensate reservoirs. J. Pet. Tech. *39*, 981–998 (1987).

[12] Li, B., Chen, Z., Huan, G.: The sequential method for the black oil model on unstructured grids. J. Comput. Phys. *192*, 36–72 (2003).
[13] Li, B., Chen, Z., Huan, G.: Comparison of solution schemes for black oil reservoir simulations with unstructured grids. Comp. Meth. Appl. Mech. Engng. *193*, 319–355 (2004).
[14] MacDonald, R. C., Coats, K. H.: Methods for numerical simulation of water and gas coning. Trans. SPE AIME *249*, 425–436 (1970).
[15] Nolen, J. S.: Numerical simulation of compositional phenomena in petroleum reservoirs. Reprint Series, SPE, Dallas, *11*, 268–284 (1973).
[16] Peaceman, D. W.: Interpretation of well-block pressures in numerical reservoir simulation, SPE 6893. 52nd Annual Fall Technical Conf. and Exhibition, Denver 1977.
[17] Peng, D. Y., Robinson, D. B.: A new two-constant equation of state. Ind. Eng. Chem. Fund. *15*, 59–64 (1976).
[18] Huan, G., Chen, Z., Li, B.: Applications of the control volume function approximation method to reservoir simulations. Fluid flows and transport in porous media. Mathematical and numerical treatment. In: Contemporary mathematics, Vol. 295 (Chen, Z., Ewing, R. E., eds.). AMS, 2002, pp. 279–292.
[19] Saad, Y., Schultz, M. H.: GMRES: a generalized minimal residual algorithm for solving nonsymmetric linear systems. SIAM J. Sci. Stat. Comput. *7*, 856–869 (1986).
[20] Trangenstein, J. A., Bell, J. B.: Mathematical structure of compositional reservoir simulation. SIAM J. Sci. Stat. Comput. *10*, 817–845 (1989).
[21] Verma, S., Aziz, K.A.: Control volume scheme for flexible grids in reservoir simulation, paper SPE37999. 1997 SPE Symp. on Reservoir Simulation, Dallas, June 8–11, 1997.
[22] Vinsome, P. W.: ORTHOMIN: An iterative method for solving sparse sets of simultaneous linear equations. Paper SPE 5729, presented at the SPE Symp. on Reservoir Simulation Los Angelos, California, February 19–20, 1976.
[23] Young, L. C., Stephenson, R. E.: A generalized compositional approach for reservoir simulation. Soc. Pet. Eng. J. *23*, 727–742 (1983).

Z. Chen and G. Huan
Southern Methodist University
Department of Mathematics
Dallas, TX 75275-0156, USA
e-mails: {zchen; ghuan}@mail.smu.edu

H. Wang
Research Institute of Petroleum Exploration
and Development
20 Xueyuan Road
Beijing 100083, P.R. China
e-mail: whm@petrochina.com.cn